A Digital Twin Architecture for Wireless Networked Adaptive Active Noise Control

Chuang Shi, Feiyu Du, and Qianyang Wu

***Abstract*—The active noise control (ANC) is a complementary technique to the passive noise control (PNC) to reduce the low frequency noise. The ANC controller can be implemented by pre-trained filters or adaptive filters. The adaptive ANC controller is advantageous in its adaptation to environmental changes. However, the algorithm complexity of the adaptive ANC controller increases with the scale of ANC applications, making it difficult to be carried out on low-cost processors. To resolve this problem, cloud computing should be utilized in ANC systems, and thus the wireless networked ANC system is proposed. Since it is crucial for ANC controllers to generate the anti-noise wave in real time, this paper formulates a digital twin architecture that implements the control filter adaptation in the cloud and the anti-noise signal generation on the local controller, respectively. A digital twin filtered-reference least mean squares (DT-FxLMS) algorithm is proposed to coordinate the digital twin with the local controller. Simulation and experiment results demonstrate the effectiveness and efficiency of the wireless networked ANC system based on the digital twin architecture.**

***Index Terms*—Active noise control, networked control systems, wireless sensor network, digital twin, human-centered computing**

I. Introduction

A recent study by the World Health Organisation (WHO) concluded that noise pollution has become one of the top environmental hazards to both physical health and mental wellbeing in the European region [1]. The impact and risk of noise pollution is even more severe in developing countries. Prolonged exposure to loud noises may cause people to feel stressed, annoyed, and suffer from sleep deprivation and hearing loss [2]. These facts emphasize the pressing issue regarding the development of noise monitoring and control measures.

With the rapid development of the Internet of things (IoT), noise can be monitored and visualized in both long term and real time [3]–[5]. Traditional manual collection has been replaced by acoustic sensor networks (ASNs) for higher granularity of noise data in both space and time [6]–[8]. Substantial amount of noise data and dedicated ASN node equipment have leveraged artificial intelligence for noise mapping and analyzing. For example, in a sensing and analytical system, computational methods are developed to automatically detect specific types of sound sources by machine hearing [9], [10]. The output of such a system places emphasis on the hard data evidence for inspection crews to be efficiently allocated and restriction of operation time to be precisely set.

On the other hand, noise control measures have also been extensively studied. They can be categorized into passive noise control (PNC) and active noise control (ANC). The PNC is effective in reducing high frequency noises [11], [12]. Recently, sonic crystals, which consist of periodic arrays of scatters, are employed in sound barriers to attenuate the transmission of sound at certain frequency bands [13]. When the noise frequency is low, the size, weight and cost of PNC measures may increase dramatically [14]. As a complementary technique to the PNC, the ANC tackles low frequency noise problems based on the principle of acoustic wave superposition [15]. The ANC system generates an anti-noise wave that has the same amplitude but reverse phase of the noise wave.

ANC systems are further categorized into the feedforward and feedback structures. The feedforward ANC (FFANC) system is composed of reference microphones, secondary loudspeakers, a controller and optional error microphones. The controller generates control signals according to the reference signals measured by the reference microphones. The secondary loudspeakers transmit the control signals to form the anti-noise wave. The FFANC controller can be implemented by pre-trained analog filters, pre-trained digital filters, or adaptive filters. In the case of adaptive filters, error microphones observe the superposition of the noise wave and the anti-noise wave, and provide the error signals to update the filter coefficients, as shown in Fig. 1(a). Otherwise, the error microphones can be omitted from the FFANC system.

The feedback ANC (FBANC) system has no reference microphones. The error microphones must be included in the FBANC system. The reference signals are estimated from the error signals. Therefore, the FBANC system results in notable noise attenuation with linear predictable noises, but it provides limited noise reduction performance with broadband noises. Similarly, the FBANC controller is optional to be implemented by adaptive filters, as shown in Fig. 1(b). In both the FFANC and FBANC systems, the adaptive ANC controller is advantageous in its adaptation to environmental changes and disadvantageous in its algorithm complexity, as compared to the pre-trained filter [16].

The filtered-reference least mean squares (FxLMS) is widely recognized as the standard adaptive filtering algorithm for ANC systems [17]–[19]. It converges to achieve the minimum Euclidean norm of the error signals. This results in the formation of quiet zones at the locations of the error microphones. Research has been extensively carried out to im-

This manuscript is supported jointly by the National Natural Science Foundation of China and the Civil Aviation Administration of China (Joint Grant No. U1933127).

The authors are with the School of Information and Communication Engineering, University of Electronic Science and Technology of China, Chengdu, China.

Corresponding author's email: shichuang@uestc.edu.cn

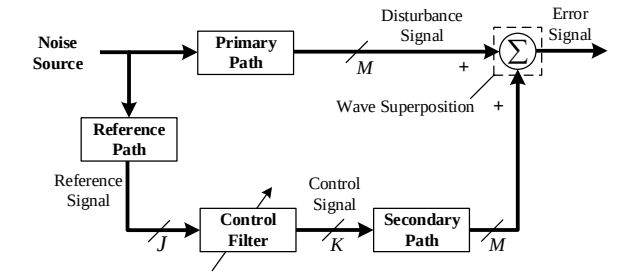

(a) Feedforward ANC structure with J reference microphones, K secondary loudspeakers, and M error microphones.

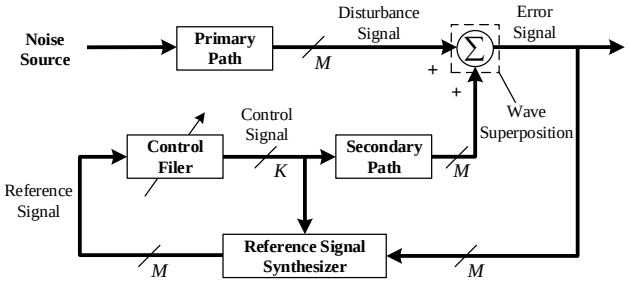

(b) Feedback ANC structure with K secondary loudspeakers and M error microphones.

Fig. 1. Typical structures of adaptive ANC systems.

prove the convergence performance of the FxLMS algorithm by means of frequency-domain, subband and block processing [20]–[24]. However, the improvement in convergence often comes at a cost of algorithm complexity. When the quiet zones are necessarily large in applications such as noise cancelling cases and active windows, even the standard FxLMS algorithm has to be implemented on costly high-performance controllers [25]–[28]. It is because the computational complexity increases dramatically with the scale of control filters, secondary path models and filtered reference signals. In contrast, the noise cancelling headphone, as one of the most mature ANC applications, still adopts the pre-trained filter, due to the scarcity of computing resources in the mobile device [29], [30].

To resolve the aforementioned problem, cloud computing, which provides almost unlimited centralized computing resources, should be utilized in ANC systems. With the rapid development of wireless communication technologies, such as the fifth generation of cellular networks (5G), that enables much reliable data transmission at a significantly lower latency, a technical trend of control systems with their sensing data being transmitted through wireless communication networks is observed [31]–[33]. Wireless communication technologies and cloud computing are combined to create the wireless networked control system, where the local controller is being moved to the cloud side [34]–[37]. The wireless networked ANC system proposed in this paper is therefore viable and highly possible.

So far, there have been few works carried out to integrate wireless communications into ANC. In 2015, Galambos and Sujbert proposed an ANC system with the concept of IoT. In their proposed system, the reference signals were transferred through the Ethernet network, which was not wireless [38]. The network latency was approximately 3 milliseconds by using the user datagram protocol (UDP). When the sound propagation from a distant noise source to the error microphone spent more time than the latency on the network, the system had adequate time to subsume all delays and play the anti-noise in time, in order for the broadband noise to be controlled. In 2018, Shen *et al.* proposed a wireless noise cancellation system, namely MUTE [39]. The core idea was similar to the previous work in [38], but emphasis was placed on the wireless relay design, in which an analog frequency modulator was adopted to bypass delays from digitization and processing. In 2021, Shen *et al.* worked out a coherence-based selection algorithm of wireless reference microphones when there were two distant noise sources operating at different times [40]. In their work, the wireless relay and the motivation of employing the wireless reference microphone were fundamentally similar to the MUTE system.

Because the secondary path model plays an essential role in ANC, the works on the wireless error microphone are few and far between. In as early as 2006, Sujbert *et al.* studied a dual-channel FBANC system, where the error signals were sampled individually and transferred over ZigBee radios [41]. They pointed out that unsynchronized sampling frequencies of the error signals led to severe modeling errors of the secondary paths. A simple unit delay might cause the ANC system to be unstable when the noise frequency was greater than a quarter of the sampling frequency. The discussion on the wireless error microphone was followed up by Shi *et al.* in 2020 [42]. They examined the use of a wireless error microphone in a single-channel FFANC system, whereby a simultaneous variable perturbation method was proposed to cope with the randomly delayed secondary path resultant from the wireless local-area network (WLAN), of which the averaged latency was about 4 milliseconds.

In summary, the network latency in transmitting the reference signal may cause failure of the ANC controller, when the noise source is not sufficiently distant or there is no dedicated wireless relay. On the other hand, the network latency in transmitting the error signal can interrupt the adaptation of the control filter. Since it is crucial for the wireless networked ANC system to generate the anti-noise wave in real time [43], it is more practical for common types of wireless communications, such as ZigBee, WLAN, 5G etc., to take place in the adaptation of the control filter instead of in the generation of the anti-noise wave. Moreover, the adaptation of the control filter can exploit digital twin to improve its stability [44]–[46], whereby a digital counterpart of the electro-acoustic relation of the ANC system is built by utilizing cloud computing.

Therefore, this paper formulates a digital twin architecture that implements the control filter adaptation in the cloud and the anti-noise signal generation on the local controller, respectively. The sensing data is collected by the local controller and uploaded into the cloud. A digital twin of the ANC system is established in the cloud, and a dedicated digital twin FxLMS (DT-FxLMS) algorithm is proposed to coordinate the digital twin with the local controller. The digital twin simulates the noise reduction process of the local controller

while adapting the control filter to its optimum solution by the DT-FxLMS algorithm. The optimized control filter coefficients are downloaded to the local controller to achieve a higher noise reduction level in the physical world. Prototypes of the wireless networked FFANC and FBANC systems are constructed based on the Cortex-M-based micro-controller with a WiFi module. Experiment results demonstrate the convergence and adaptation of the wireless networked FFANC and FBANC systems based on the digital twin architecture.

II. Theory and Method

A. Standard FxLMS Algorithm of FFANC and FBANC Systems

The structure of an FFANC system is shown in Fig. 1 (a). At time n, the reference microphone obtains a reference signal $x(n)$, which is stored in a vector form as

$$\mathbf{x}(n) = [x(n), x(n-1), \ldots, x(n-N+1)], \tag{1}$$

where N is the tap length of the control filter.

The control filter $\mathbf{w}(n)$ takes in the reference signal and output the control signal $y(n)$, *i.e.*

$$y(n) = \mathbf{w}(n)\mathbf{x}^T(n), \tag{2}$$

where the superscript T denotes the transpose operation.

The primary path $\mathbf{p}(n)$ is defined as the acoustic path and the effects of the electro-acoustic devices from the reference microphone to the error microphone. It can be considered as a system that takes in the reference signal and outputs the disturbance wave $d(n)$, which is written as

$$d(n) = \mathbf{p}(n)\mathbf{x}^T(n). \tag{3}$$

It is of significance to note that $\mathbf{p}(n)$ is always unknown to ANC systems.

Similar to the primary path, the secondary path $\mathbf{s}(n)$ is composed of the acoustic path and the effects of the electro-acoustic devices between the secondary loudspeaker and the error microphone. It takes the control signal as the input and generates the anti-noise wave $y'(n)$ as the output, *i.e.*

$$y'(n) = \mathbf{s}(n)\mathbf{y}^T(n), \tag{4}$$

where

$$\mathbf{y}(n) = [y(n), y(n-1), \ldots, y(n-N_s+1)] \tag{5}$$

and N_s is the length of the secondary path model.

The error signal $e(n)$ measures the superposition of the disturbance wave and the anti-noise wave, which can be written as

$$e(n) = d(n) + y'(n). \tag{6}$$

In the standard FxLMS algorithm, the filtered reference signal is the output of the secondary path model $\hat{\mathbf{s}}(n)$ when its input is the reference signal. It is written as

$$r(n) = \hat{\mathbf{s}}(n)\mathbf{x}^T(n), \tag{7}$$

where $\hat{\mathbf{s}}(n)$ is an estimate of the true secondary path $\mathbf{s}(n)$.

Thereafter, the control filter coefficients are updated by

$$\mathbf{w}(n+1) = \mathbf{w}(n) - \mu e(n)\mathbf{r}(n), \tag{8}$$

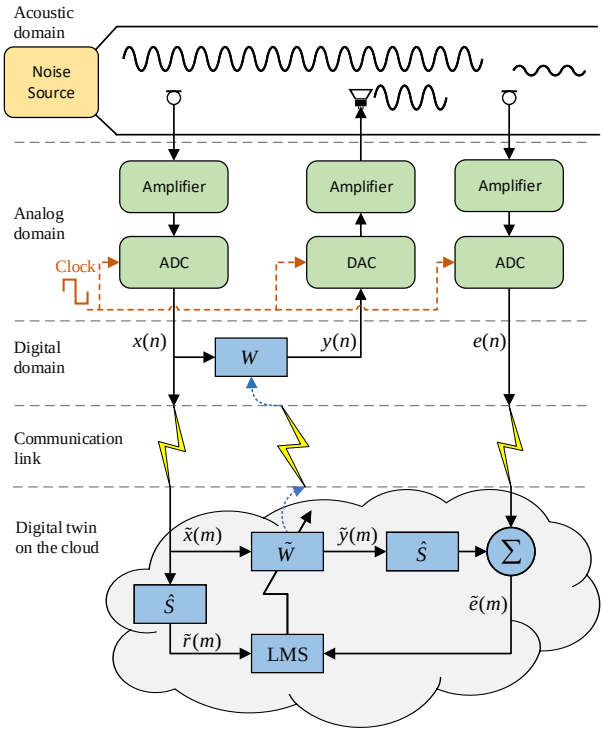

Fig. 2. Digital twin architecture of the FFANC system.

where μ is the step size; and $\mathbf{r}(n)$ is the vector form of the filtered reference signal, which can be written as

$$\mathbf{r}(n) = [r(n), r(n-1), \ldots, r(n-N+1)]. \tag{9}$$

The structure of an FBANC system is shown in Fig. 1 (b). Since there is no reference microphone, the reference signal is estimated from the error signal as

$$x(n) = e(n) - \hat{\mathbf{s}}(n)\mathbf{y}^T(n). \tag{10}$$

In the FxLMS algorithm for the FBANC system, generation of the control signal, calculation of the filtered reference signal, and updating the control filter coefficients are identical to (2), (7) and (8), respectively.

B. Digital Twin Architecture of FFANC and FBANC Systems

As shown in Fig. 2, the digital twin architecture of the FFANC system is composed of the local controller, the network communication, and the digital twin in the cloud. The local controller is a typical FFANC controller, including the acoustic domain, analog domain, and digital domain. Noise and anti-noise waves interfere with each other in the acoustic domain. Sound pressures are converted into digital signals in the analog domain by the analog-to-digital converter (ADC) and vice versa by the digital-to-analog converter (DAC). Signal processing takes place in the digital domain. The DT-FxLMS algorithm is proposed to coordinate the digital twin in the cloud with the local controller as follows.

The reference and error signals are buffered in the local controller as

$$\mathbf{x}_L(n) = [x(n), x(n-1), \ldots, x(n-L+1)] \tag{11}$$

and

$$\mathbf{e}_L(n) = [e(n), e(n-1), \ldots, e(n-L+1)], \quad (12)$$

where L is the buffer size. If the buffer is filled up at time n, $\mathbf{x}_L(n)$ and $\mathbf{e}_L(n)$ are uploaded into the cloud. Thereafter, the digital twin starts its simulation.

Let the time index m range from $n+N-L$ to n in the digital twin. Therefore, at an arbitrary time m, the reference signal $\widetilde{\mathbf{x}}(m)$ in the digital twin is able to be written as

$$\widetilde{\mathbf{x}}(m) = [x(m), x(m-1), \ldots, x(m-N+1)]. \quad (13)$$

The error signal $\widetilde{e}(m)$ in the digital twin is calculated by

$$\widetilde{e}(m) = e(m) + \hat{\mathbf{s}}(m)\widetilde{\mathbf{y}}^T(m), \quad (14)$$

where

$$\widetilde{\mathbf{y}}(m) = [\widetilde{y}(m), \widetilde{y}(m-1), \ldots, \widetilde{y}(m-N_s+1)] \quad (15)$$

and

$$\widetilde{y}(m) = \widetilde{\mathbf{w}}(m)\widetilde{\mathbf{x}}^T(m). \quad (16)$$

Here, $\widetilde{\mathbf{w}}(m)$ denotes the control filter in the digital twin, which is initialized as a zero vector at time $m = n+N-L$.

The filtered reference signal is calculated by

$$\widetilde{r}(m) = \hat{\mathbf{s}}(m)\widetilde{\mathbf{x}}^T(m). \quad (17)$$

The vector form of the filtered reference signal in the digital twin can be written as

$$\widetilde{\mathbf{r}}(m) = [\widetilde{r}(m), \widetilde{r}(m-1), \ldots, \widetilde{r}(m-N+1)]. \quad (18)$$

Therefore, the control filter coefficients are updated in the digital twin as

$$\widetilde{\mathbf{w}}(m+1) = \widetilde{\mathbf{w}}(m) - \mu\widetilde{e}(m)\widetilde{\mathbf{r}}(m). \quad (19)$$

To ensure the convergence of the control filter, the buffer size should be sufficiently longer than the tap length of the control filter.

At time $m = n$, the simulation completes in the digital twin. The control filter coefficients are downloaded to the local controller as the incremental vector. Therefore, local controller updates its control filter coefficients by

$$\mathbf{w}(n'+1) = \mathbf{w}(n') + \widetilde{\mathbf{w}}(n+1), \quad (20)$$

where n' is the current time index in the local controller and the buffers of the reference and error signals are reset at the same time.

Similarly, as shown in Fig. 3, the digital twin architecture of the FBANC system is also composed of the local controller, the network communication, and the digital twin in the cloud. The local controller receives the error signal from the analog domain and outputs the control signal. In the digital domain, the local controller firstly calculates the reference signal and then generates the control signal by the control filter. The computational complexity on the local FBANC controller is thus higher than that on the local FFANC controller.

As long as the calculated reference and error signals are buffered in the local controller together as (11) and (12), the digital twin in the cloud need not distinguish the FFANC and FBANC systems. The DT-FxLMS algorithm remains the same in the cloud. Once the simulation is completed in the digital twin, the incremental vector is downloaded to the local controller and updates the control filter coefficients as (20) too.

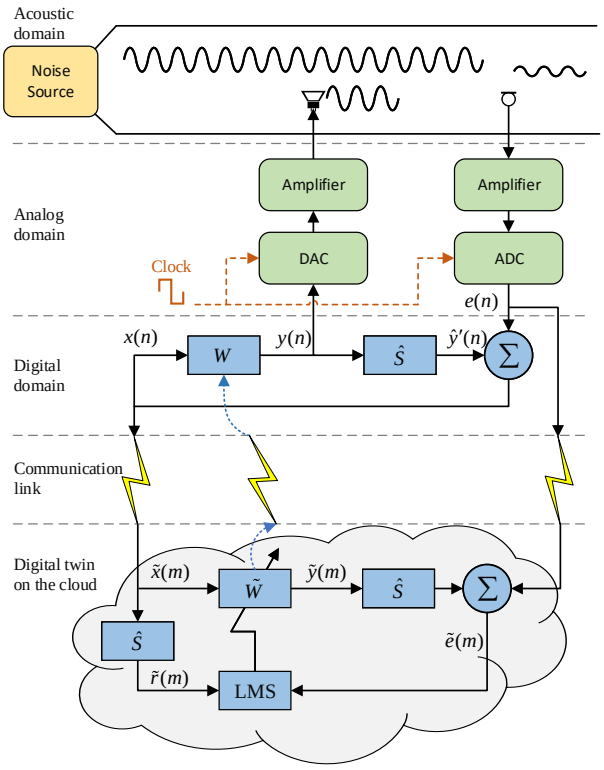

Fig. 3. Digital twin architecture of the FBANC system.

By using the DT-FxLMS algorithm, the local controller is set free from calculating the filtered reference signal and updating the control filter coefficients. The local controller only needs to generate the control signal in real time and upload the sensing data to the cloud. Therefore, the computational complexity of the DT-FxLMS algorithm on the local controller is almost the same as using the pre-trained digital filter.

C. Convergence Analysis of the DT-FxLMS Algorithm

According to the steady-state solution of the FxLMS algorithm [47], the control filter coefficients in the local controller are presumed to converge to $\mathbf{w}(\infty)$, satisfying

$$E[d(n)\widetilde{\mathbf{r}}(n) + \mathbf{w}(\infty)\mathbf{r}_0^T(n)\widetilde{\mathbf{r}}(n)] = 0, \quad (21)$$

where

$$\mathbf{r}_0(n) = [r_0(n), r_0(n-1), \ldots, r_0(n-N+1)] \quad (22)$$

and

$$r_0(n) = \mathbf{s}(n)\mathbf{x}^T(n). \quad (23)$$

Subtracting $\mathbf{w}(\infty)$ from both sides of (20) yields

$$\Delta\mathbf{w}(n'+1) = \Delta\mathbf{w}(n') + \widetilde{\mathbf{w}}(n+1), \quad (24)$$

where $\Delta\mathbf{w}(n') = \mathbf{w}(n') - \mathbf{w}(\infty)$.

Taking expectations of both sides of (24) yields

$$E[\Delta\mathbf{w}(n'+1)] = E[\Delta\mathbf{w}(n')] + E[\widetilde{\mathbf{w}}(n+1)]. \quad (25)$$

The DT-FxLMS algorithm can lead to a steady-state solution on the local controller, only if $E[\widetilde{\mathbf{w}}(n+1)]$ converges in the cloud in the first place.

Therefore, taking expectations of both sides of (19) yields

$$E[\widetilde{\mathbf{w}}(m+1)] = E[\widetilde{\mathbf{w}}(m)] - \mu E[\widetilde{e}(m)\widetilde{\mathbf{r}}(m)]. \quad (26)$$

For analysing the last term in (26), substituting (4) and (6) into (14) yields

$$\begin{aligned}\widetilde{e}(m) &= d(m) + \mathbf{s}(m)\mathbf{y}^T(m) + \hat{\mathbf{s}}(m)\widetilde{\mathbf{y}}^T(m) \\ &= d(m) + \mathbf{w}(m)\mathbf{r}_0^T(m) + \widetilde{\mathbf{w}}(m)\widetilde{\mathbf{r}}^T(m). \end{aligned} \quad (27)$$

The slow adaptation assumption is adopted here, in order for the control filter to swap with the secondary path or the secondary path model when the reference signal is treated as the input of two cascaded linear time-invariant systems.

Both $\mathbf{w}(m)$ and $\widetilde{\mathbf{w}}(m)$ are assumed to be statistically independent from $\mathbf{r}_0(m)$ and $\widetilde{\mathbf{r}}(m)$. Using (21) and $\mathbf{w}(m) = \mathbf{w}(\infty) + \Delta\mathbf{w}(m)$ yields

$$E[\widetilde{e}(m)\widetilde{\mathbf{r}}(m)] = E[\Delta\mathbf{w}(m)]\mathbf{R}_{r_0\widetilde{r}} + E[\widetilde{\mathbf{w}}(m)]\mathbf{R}_{\widetilde{r}\widetilde{r}}, \quad (28)$$

where $\mathbf{R}_{r_0\widetilde{r}} = E[\mathbf{r}_0^T(m)\widetilde{\mathbf{r}}(m)]$ and $\mathbf{R}_{\widetilde{r}\widetilde{r}} = E[\widetilde{\mathbf{r}}^T(m)\widetilde{\mathbf{r}}(m)]$.

Substituting (28) into (26) yields

$$E[\widetilde{\mathbf{w}}(m+1)] = E[\widetilde{\mathbf{w}}(m)]\mathbf{U} + \mathbf{V}, \quad (29)$$

where

$$\mathbf{U} = \mathbf{I} - \mu\mathbf{R}_{\widetilde{r}\widetilde{r}} \quad (30)$$

and

$$\mathbf{V} = -\mu E[\Delta\mathbf{w}(m)]\mathbf{R}_{r_0\widetilde{r}}. \quad (31)$$

When the largest eigenvalue of $\mathbf{U}$ is less than 1, *i.e.* $\lambda_{\max}\{\mathbf{U}\} < 1$, (29) becomes a simple iteration. Since $\mathbf{R}_{\widetilde{r}\widetilde{r}}$ is positive definite, the above mentioned condition is equivalent to

$$0 < \mu < \frac{2}{\lambda_{\max}\{\mathbf{R}_{\widetilde{\mathbf{r}}\widetilde{\mathbf{r}}}\}}, \quad (32)$$

where $\lambda_{\max}(\cdot)$ denotes the largest eigenvalue of a matrix.

The fixed point of the simple iteration provides

$$E[\widetilde{\mathbf{w}}(m+1)] = \mathbf{V}(\mathbf{I}-\mathbf{U})^{-1} = -E[\Delta\mathbf{w}(m)]\mathbf{R}_{r_0\widetilde{r}}\mathbf{R}_{\widetilde{r}\widetilde{r}}^{-1}. \quad (33)$$

Letting $m = n$ in (33) and substituting it into (25) yields

$$E[\Delta\mathbf{w}(n'+1)] = E[\Delta\mathbf{w}(n')] - E[\Delta\mathbf{w}(n)]\mathbf{R}_{r_0\widetilde{r}}\mathbf{R}_{\widetilde{r}\widetilde{r}}^{-1}. \quad (34)$$

Since the local controller does not update the control filter coefficients from time n until time n', $E[\Delta\mathbf{w}(n')] = E[\Delta\mathbf{w}(n)]$ is valid.

Therefore, (34) becomes another simple iteration, *i.e.*

$$E[\Delta\mathbf{w}(n'+1)] = E[\Delta\mathbf{w}(n')](\mathbf{I} - \mathbf{R}_{r_0\widetilde{r}}\mathbf{R}_{\widetilde{r}\widetilde{r}}^{-1}), \quad (35)$$

which converges to a zero vector when

$$-\mathbf{I} < \mathbf{I} - \mathbf{R}_{r_0\widetilde{r}}\mathbf{R}_{\widetilde{r}\widetilde{r}}^{-1} < \mathbf{I}. \quad (36)$$

This convergence condition can be further written as

$$\mathbf{O} < \mathbf{R}_{r_0\widetilde{r}} < 2\mathbf{R}_{\widetilde{r}\widetilde{r}}. \quad (37)$$

It is worth noting that the duration from n to n' is the total time consumed to complete the digital twin simulation in the cloud and to communicate between the local controller and the cloud. This duration does not affect the convergence of the DT-FxLMS algorithm, as long as the accuracy of the secondary path model satisfies (37). The downside of the DT-FxLMS algorithm is found in its slower convergence speed and less timely update of the control filter, as compared to the FxLMS algorithm.

Furthermore, when $\widetilde{\mathbf{r}}$ is replaced by $\mathbf{r}$ in the convergence analysis, (21) and (37) become identical to those of the FxLMS algorithm. They validate that the DT-FxLMS algorithm can converge to the same steady-state solution as the FxLMS algorithm in theory.

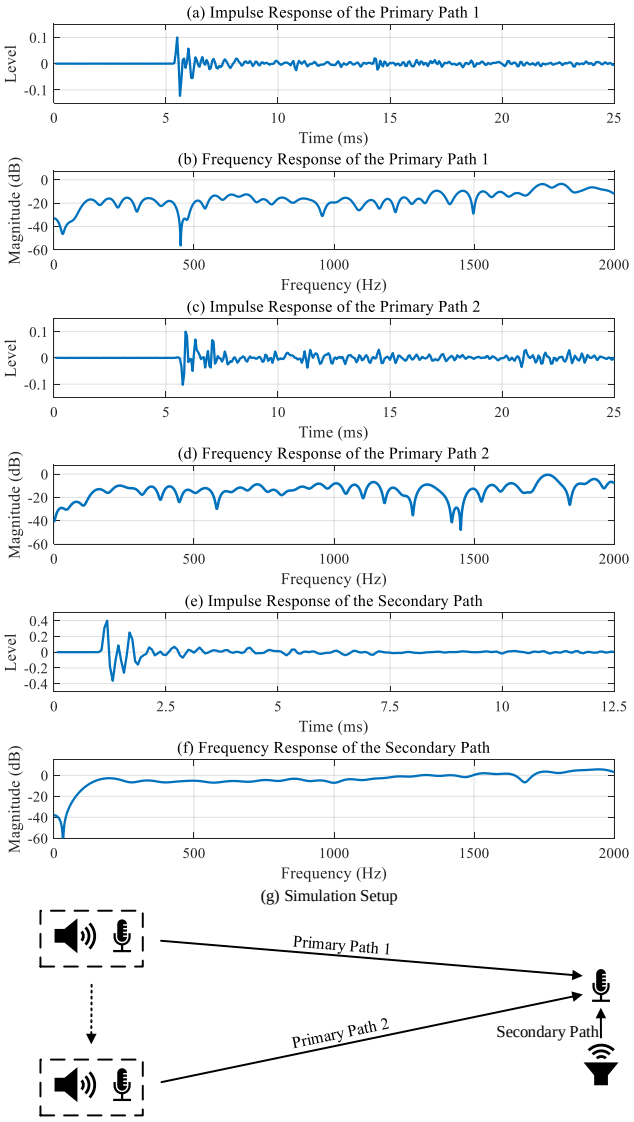

Fig. 4. Primary and secondary paths for the single-channel ANC simulation.

III. Simulation Results

Simulations were carried out with a single-channel ANC system setup, of which the primary and secondary paths were measured in advance. Their impulse responses and frequency responses are shown in Fig. 4, along with the measurement

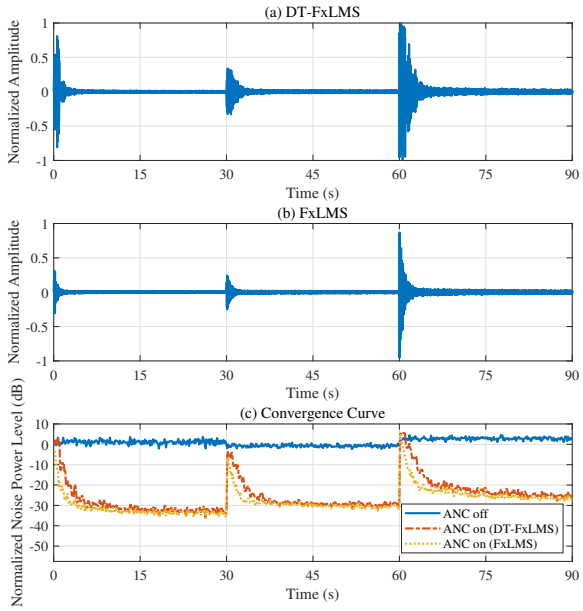

Fig. 5. Simulated error signals of the FFANC system using the FxLMS and DT-FxLMS algorithms.

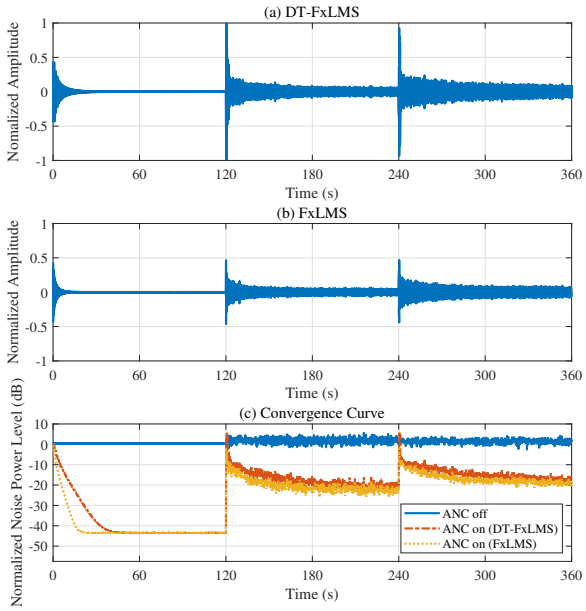

Fig. 7. Simulated error signals of the FBANC system using the FxLMS and DT-FxLMS algorithms.

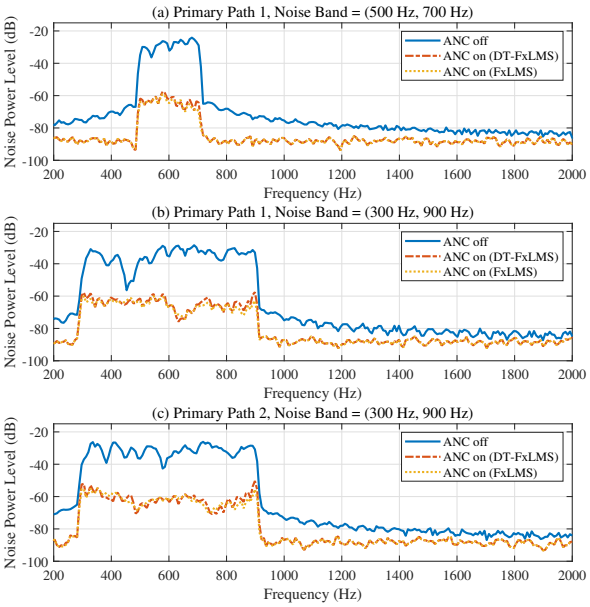

Fig. 6. Simulated noise spectra of the FFANC system using the FxLMS and DT-FxLMS algorithms.

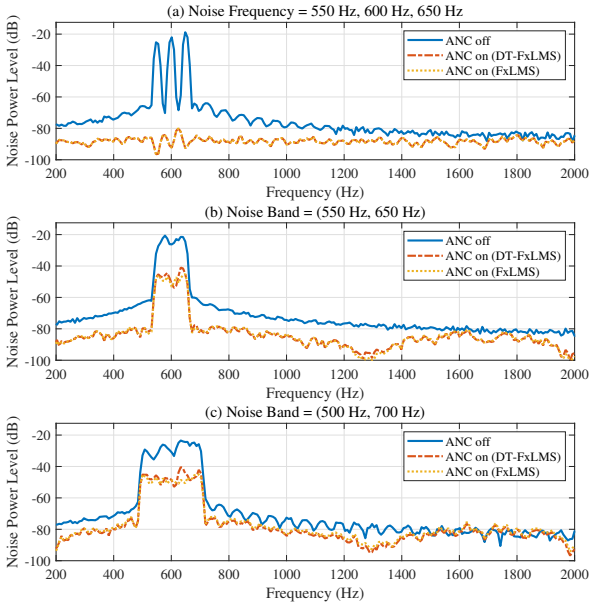

Fig. 8. Simulated noise spectra of the FBANC system using the FxLMS and DT-FxLMS algorithms.

setup. The noise source was placed at two different locations to create two primary paths. The simulation was initialized with the primary path 1 and shifted to the primary path 2 in a latter stage to demonstrate the adaptivity of the wireless networked adaptive ANC system. The sampling rate was set to $f_s = 16$ kHz. The lengths of the control filter and the secondary path model were set to $N = 400$ taps and $N_s = 200$ taps, respectively. The buffer size was $L = 8000$ taps. A noise floor was added to the error microphone by a white Gaussian noise with the normalized power of 1.

Figure 5 shows the error signals of the conventional FFANC system using the FxLMS algorithm and the wireless networked FFANC system using the DT-FxLMS algorithm. The same step size $\mu = 0.01/\|\mathbf{x}(n)\|_2^2$ was used for both algorithms. This step size ensured the convergence of both algorithms, while letting the difference in their convergence speeds be

easily observed. In the first 30 seconds of the simulation, the primary path 1 was adopted and the noise source was a band-limited noise from 500 Hz to 700 Hz. The power of this band-limited noise was 45.0 dB higher than the noise floor. From 30 seconds to 60 seconds of the simulation, the noise source was changed to another band-limited noise from 300 Hz to 900 Hz. The power of this band-limited noise was 43.1 dB higher than the noise floor. In the last 30 seconds of the simulation, the primary path 2 was adopted and the noise frequency remained in the range of 300 Hz to 900 Hz. As a result of changing the primary path, the power of the band-limited noise increased to 46.6 dB higher than the noise floor. Both the FxLMS and DT-FxLMS algorithms converged to control filters that generate the effective anti-noise signals. The convergence process of the DT-FxLMS algorithm was slower and less smooth than the FxLMS algorithm. Figure 6 shows the power spectra of the error signals. Although the communication between the local controller and the cloud only took place every time the buffer was filled up, the steady-state performance of the DT-FxLMS algorithm was not affected. The DT-FxLMS algorithm converged to almost the same steady state as compared to the FxLMS algorithm in all three stages of the simulation.

Figure 7 shows the error signals of the conventional FBANC system using the FxLMS algorithm and the wireless networked FBANC system using the DT-FxLMS algorithm. Only the primary path 1 was adopted. In the first 120 seconds of the simulation, the noise source was a multi-tonal noise, consisting of 550 Hz, 600 Hz and 650 Hz sinusoid waves. From 120 seconds to 240 seconds of the simulation, the noise source was changed to a narrow band noise, of which the frequency ranged from 550 Hz to 650 Hz. In the last 120 seconds of the simulation, the noise source changed to a relative broad band noise, of which the frequency ranged from 500 Hz to 700 Hz. The step size was set to $\mu = 0.001/\|\mathbf{x}(n)\|_2^2$, $\mu = 0.01/\|\mathbf{x}(n)\|_2^2$ and $\mu = 0.02/\|\mathbf{x}(n)\|_2^2$ in three stages of the simulation, respectively. The smallest step size was used for the primary noise with the narrowest bandwidth. Otherwise, the converge processes of both algorithms would be too short to demonstrate that the DT-FxLMS algorithm was slower than the FxLMS algorithm. The power of the noise was 43.8 dB, 45.6 dB and 45.1 dB higher than the noise floor in the three stages of the simulation, respectively. Both the FxLMS and DT-FxLMS algorithms converged to control filters that generate the effective anti-noise signals. However, as compared to the FFANC simulation, the convergence speed of the DT-FxLMS algorithm became slower in the FBANC simulation. Figure 8 shows the power spectra of the error signals. The DT-FxLMS algorithm could converge to the same steady state as compared to the FxLMS algorithm in the first stage of the simulation, but led to slightly lower noise reduction levels than the FxLMS algorithm when dealing with narrow band and broad band noises.

IV. Experiment Results

Experiments of both the FFANC and FBANC systems were carried out on the Cortex-M-based micro-controller (STM32F407) with a WiFi module (ESP8266), as shown in Fig. 9. The micro-controller was implemented as the local controller. Two 1/2 inch measurement microphone sets (CRY333) were used as the reference and error microphones [48]. They were connected to or disconnected from the micro-controller's internal ADCs depending on the ANC structure. The internal DAC was used to output the control signal. Two multimedia speakers were used as the noise source and the secondary loudspeaker, respectively. A laptop was employed to play the role of the cloud side, where the digital twin ran. The UDP was adopted to communicate between the micro-controller and the laptop. The sampling rate was set to $f_s = 7114$ Hz. The lengths of the control filter and the secondary path model were set to $N = 200$ taps and $N_s = 100$ taps, respectively. As the experiment environment was not an ideal linear time-invariant system, a relatively small step size should be considered to ensure the convergence, and a sufficiently large buffer should correspondingly be employed. Therefore, the buffer size and the step size were set to $L = 10000$ taps $\mu = 0.001/\|\mathbf{x}(n)\|_2^2$, respectively.

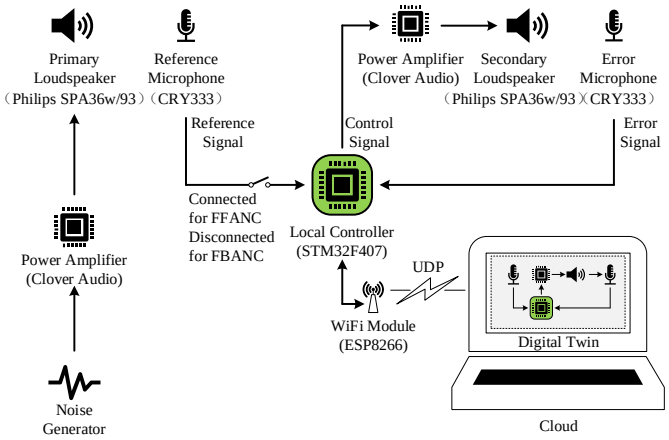

Fig. 9. Experimental setup of the wireless networked FFANC and FBANC systems.

Three band-limited noise sources were used in the experiments of the FFANC system. The first noise source ranged from 550 Hz to 650 Hz, with the sound pressure level (SPL) of 72.1 dBA. The second noise source ranged from 500 Hz to 700 Hz, with the SPL of 71.9 dBA. And the third noise source ranged from 300 Hz to 900 Hz, with the SPL of 70.2 dBA. The first two noise sources were also adopted in the experiments of the FBANC system. A multi-tonal noise source was further included, which consisted of 550 Hz, 600 Hz and 650 Hz sinusoid waves. The SPL of this multi-tonal noise source was 71.2 dBA. All the above SPLs were measured with a class 2 SPL meter (AWA5636-0) at the location of the error microphone [49]. Moreover, before any noise sources and the secondary loudspeaker were powered up, the SPL was recorded as 35.7 dBA at the location of the error microphone.

Figure 10 shows the normalized noise power levels measured by the error microphones of the conventional FFANC system and the wireless networked FFANC system. The conventional FFANC system adopted the FxLMS algorithm, and wireless networked FFANC system adopted the DT-FxLMS

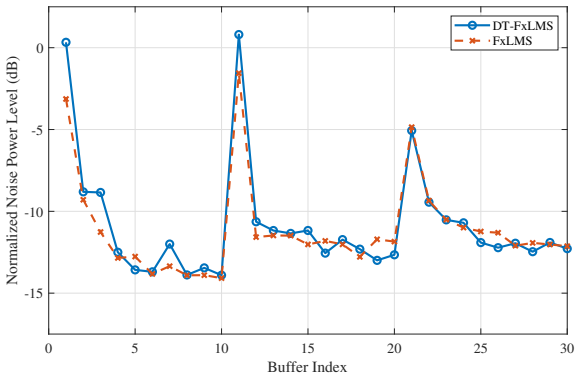

Fig. 10. Measured convergence curves of the FFANC system using the FxLMS and DT-FxLMS algorithms.

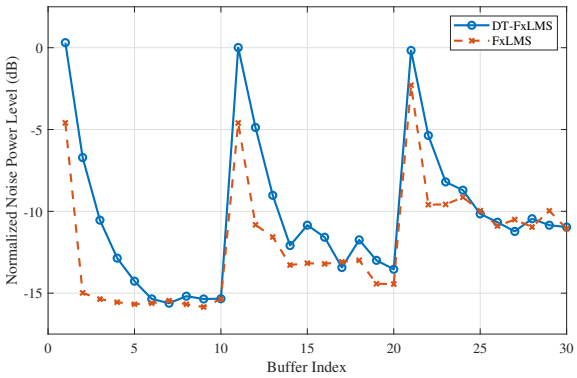

Fig. 12. Measured convergence curves of the FBANC system using the FxLMS and DT-FxLMS algorithms.

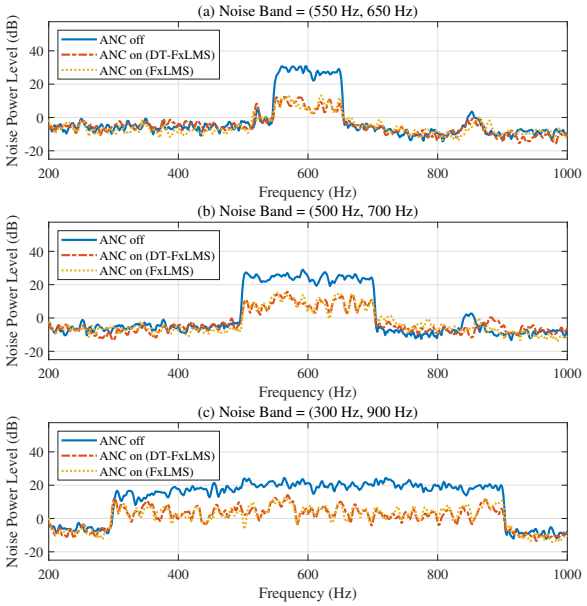

Fig. 11. Measured noise spectra of the FFANC system using the FxLMS and DT-FxLMS algorithms.

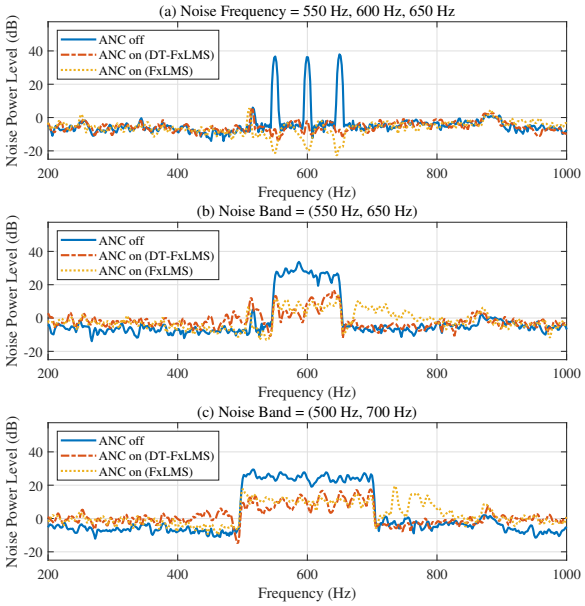

Fig. 13. Measured noise spectra of the FBANC system using the FxLMS and DT-FxLMS algorithms.

algorithm. The conventional FFANC system using the FxLMS algorithm had reduced the SPLs at the location of the error microphone by 18.4, 15.4 and 14.4 dBA in the three stages of the experiment, respectively. The wireless networked FFANC system using the DT-FxLMS algorithms had reduced the SPLs at the location of the error microphone by 17.3, 15.9 and 14.7 dBA in three stages of the experiment, respectively. The results of the DT-FxLMS algorithm were very close to the results of the FxLMS algorithm. Figure 11 shows the power spectra of the error signals. Similar to the trends in the simulation, the steady-state performance of the DT-FxLMS algorithm was also close to the FxLMS algorithm in all the three stages of the experiment.

Figure 12 shows the normalized noise power level measured by the error microphones of the conventional FBANC system and the wireless networked FBANC system. The conventional FBANC system using the FxLMS algorithm had reduced the SPLs at the location of the error microphone by 25.2, 17.3 and 12.4 dBA in three stages of the experiment, respectively. The wireless networked FBANC system using the DT-FxLMS algorithms had reduced the SPLs at the location of the error microphone by 25.2, 17.5 and 13.4 dBA in three stages of the experiment, respectively. The convergence speed of the DT-FxLMS algorithm became slower than the FxLMS algorithm, when the noise source was a multi-tonal noise. Figure 13 shows the power spectra of the error signals. The DT-FxLMS algorithm converged to very close noise reduction levels, but led to different water bed effects, as compared to the FxLMS algorithm.

Lastly, Table I lists the computational loads of two algorithms on the local controller. The computational loads are counted by the number of multiply accumulators (MACs). The

TABLE I
COMPUTATIONAL LOADS OF THE DT-FXLMS AND FXLMS ALGORITHM ON THE LOCAL CONTROLLER

Algorithm	FFANC (DT-FxLMS)	FFANC (FxLMS)	FBANC (DT-FxLMS)	FBANC (FxLMS)
Estimation of the reference signal	-	-	N_s MACs	N_s MACs
Generation of the control signal	N MACs	N MACs	N MACs	N MACs
Adaptation of the control filter	-	$N + N_s$ MACs	-	$N + N_s$ MACs
In Total (C_{total})	N MACs	$2N + N_s$ MACs	$N + N_s$ MACs	$2N + 2N_s$ MACs

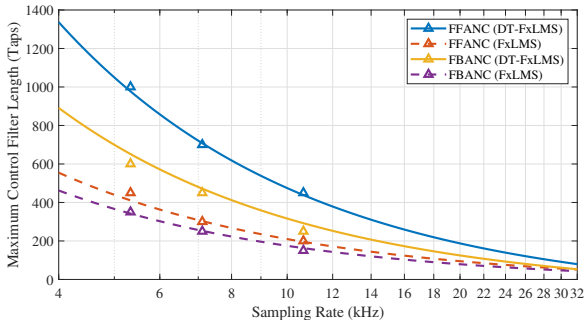

Fig. 14. Maximum lengths of the control filters in the FFANC and FBANC systems using different sampling rates.

relation between the sampling rate and the computational load is described by

$$\frac{1}{f_s} \geq t_0(C_{total} + C_{overhead}), \tag{38}$$

where t_0 denotes the executing time of a MAC, which was 0.174 us in the experiment; C_{total} denotes the total computation load of an algorithm, as listed in Table 1; and $C_{overhead}$ denotes the equivalent number of MACs of the overhead, which includes the data communication, ADC, DAC, and so on. It should be noted that the network latency is not part of the overhead. The network latency only affects the timeliness of the control filter adaptation and does not cause the ANC controller to fail. In the experiment of this paper, logging the noise power level was counted into the overhead. Therefore, the equivalent number of MACs were approximated as 100 MACs and 50 MACs for the overheads of the DT-FxLMS and FxLMS algorithms, respectively.

Figure 14 shows maximum lengths of the control filters (for $N_s = 0.5 \times N$) in the FFANC and FBANC systems using different sampling rates, where the lines represent the theoretical predictions by (38) and the triangle markers represent the measured results. Due to the restrictions of the STM32F407, the sampling rate can only be set to discrete values, such as 5335 Hz, 7114 Hz, 10671 Hz, etc. Based on the measured results, the DT-FxLMS algorithm achieves more than twice the length of the control filter in the FFANC system, as compared to the FxLMS algorithm. The advantage of the DT-FxLMS is less significant in the FBANC system, as the computational complexity on the local FBANC controller is higher than that in the local FFANC controller. In this case, the DT-FxLMS algorithm still achieves nearly twice the length of the control filter, as compared to the FxLMS algorithm. As indicated by the theoretical predictions, with the same length of the control filter, the DT-FxLMS algorithm allows the sampling rate to be increased by about 100% and 50% as compared to the FxLMS algorithm in the FFANC and FBANC systems, respectively.

V. CONCLUSIONS

The balance of advanced algorithms and the hardware cost is a problem that has to be taken into consideration for ANC systems. Thus, this paper proposes the wireless networked ANC system to incorporate cloud computing. The wireless networked ANC system can remove a significant portion of the computational load from the local controller to ensure the generation of the anti-noise wave to be feasibly carried out in real time by a low-cost micro-controller. The sensing data is collected by the local controller and uploaded into the cloud. A digital twin of the ANC system is established in the cloud, which simulates the optimum noise reduction process of the local controller while adapting the control filter to its optimum solution by the dedicated DT-FxLMS algorithm. The optimized control filter coefficients are downloaded onto the local controller to achieve a higher noise reduction level in the physical world. Simulation and experiment results demonstrate that the steady-state performance of the DT-FxLMS algorithm is very close to the classic FxLMS algorithm in both the FFANC and FBANC systems. Hence, the wireless networked ANC system can be readily integrated with the noise monitoring ASNs in the future to provide a package solution to noise monitoring and control problems in urban and industrial applications.

REFERENCES

[1] WHO Regional Office for Europe, *Environmental Noise Guidelines for the European Region*. The Regional Office for Europe of the World Health Organization, Copenhagen, Denmark, 2018.

[2] M. S. Hammer, T. K. Swinburn, and R. L. Neitzel, "Environmental noise pollution in the United States: Developing an effective public health response," *Environmental Health Perspectives*, vol. 122, no. 2, pp. 115–119, 2014.

[3] A. Pastor-Aparicio, J. Segura-Garcia, J. Lopez-Ballester, S. Felici-Castell, M. García-Pineda, and J. J. Pérez-Solano, "Psychoacoustic annoyance implementation with wireless acoustic sensor networks for monitoring in smart cities," *IEEE Internet of Things Journal*, vol. 7, no. 1, pp. 128–136, 2020.

[4] E.-L. Tan, F. A. Karnapi, L. J. Ng, K. Ooi, and W.-S. Gan, "Extracting urban sound information for residential areas in smart cities using an end-to-end IoT system," *IEEE Internet of Things Journal*, vol. 8, no. 18, pp. 14308–14321, 2021.

[5] J. Segura-Garcia, J. M. A. Calero, A. Pastor-Aparicio, R. Marco-Alaez, S. Felici-Castell, and Q. Wang, "5G IoT system for real-time psychoacoustic soundscape monitoring in smart cities with dynamic computational offloading to the edge," *IEEE Internet of Things Journal*, vol. 8, no. 15, pp. 12467–12475, 2021.

[6] Y. Liu, X. Ma, L. Shu, Q. Yang, Y. Zhang, Z. Huo, and Z. Zhou, "Internet of Things for noise mapping in smart cities: State of the art and future directions," *IEEE Network*, vol. 34, no. 4, pp. 112–118, 2020.

[7] J. Segura-Garcia, S. Felici-Castell, J. J. Perez-Solano, M. Cobos, and J. M. Navarro, "Low-cost alternatives for urban noise nuisance monitoring using wireless sensor networks," *IEEE Sensors Journal*, vol. 15, no. 2, pp. 836–844, 2015.

[8] D. Dobrilović, V. Brtka, G. Jotanović, Ž. Stojanov, G. Jauševac, and M. Malić, "The urban traffic noise monitoring system based on LoRaWAN technology," *Wireless Networks*, vol. 28, no. 1, pp. 441–458, 2021.

[9] J. P. Bello, C. Silva, O. Nov, R. L. Dubois, A. Arora, J. Salamon, C. Mydlarz, and H. Doraiswamy, "SONYC: A system for monitoring, analyzing, and mitigating urban noise pollution," *Communications of the ACM*, vol. 62, no. 2, pp. 68–77, 2019.

[10] J. Salamon and J. P. Bello, "Deep convolutional neural networks and data augmentation for environmental sound classification," *IEEE Signal Processing Letters*, vol. 24, no. 3, pp. 279–283, 2017.

[11] G. Watts and N. Godfrey, "Effects on roadside noise levels of sound absorptive materials in noise barriers," *Applied Acoustics*, vol. 58, no. 4, pp. 385–402, 1999.

[12] B.-I. Popa, Y. Zhai, and H.-S. Kwon, "Broadband sound barriers with bianisotropic metasurfaces," *Nature Communications*, vol. 9, no. 1, pp. 5299–5299, 2018.

[13] J. Y. Hong and J. Y. Jeon, "The effects of audio–visual factors on perceptions of environmental noise barrier performance," *Landscape and Urban Planning*, vol. 125, pp. 28–37, 2014.

[14] S. M. Kuo and D. Morgan, "Active noise control: A tutorial review," *Proceedings of the IEEE*, vol. 87, no. 6, pp. 943–973, 1999.

[15] Y. Kajikawa, W.-S. Gan, and S. M. Kuo, "Recent advances on active noise control: Open issues and innovative applications," *APSIPA Transactions on Signal and Information Processing*, vol. 1, no. 1, pp. 1-21, 2012.

[16] P. N. Samarasinghe, W. Zhang, and T. D. Abhayapala, "Recent advances in active noise control inside automobile cabins: Toward quieter cars," *IEEE Signal Processing Magazine*, vol. 33, no. 6, pp. 61–73, 2016.

[17] S. Elliott, I. Stothers, and P. Nelson, "A multiple error LMS algorithm and its application to the active control of sound and vibration," *IEEE Transactions on Acoustics, Speech, and Signal Processing*, vol. 35, no. 10, pp. 1423–1434, 1987.

[18] M. Ferrer, A. Gonzalez, M. de Diego and G. Pinero, "Convex combination filtered-x algorithms for active noise control systems," *IEEE Transactions on Audio, Speech, and Language Processing*, vol. 21, no. 1, pp. 156-167, 2013.

[19] D. Shi, W.-S. Gan, B. Lam, S. Wen and X. Shen, "Optimal output-constrained active noise control based on inverse adaptive modeling leak factor estimate," *IEEE/ACM Transactions on Audio, Speech, and Language Processing*, vol. 29, pp. 1256-1269, 2021.

[20] J. Cheer and S. Daley, "An investigation of delayless subband adaptive filtering for multi-input multi-output active noise control applications," *IEEE/ACM Transactions on Audio, Speech, and Language Processing*, vol. 25, no. 2, pp. 359–373, 2017.

[21] M. Gao, J. Lu, and X. Qiu, "A simplified subband ANC algorithm without secondary path modeling," *IEEE/ACM Transactions on Audio, Speech, and Language Processing*, vol. 24, no. 7, pp. 1164–1174, 2016.

[22] D. Shi, B. Lam, W.-S. Gan, and S. Wen, "Block coordinate descent based algorithm for computational complexity reduction in multichannel active noise control system," *Mechanical Systems and Signal Processing*, vol. 151, p. 107346, 2021.

[23] F. Albu and M. Bouchard, "A low-cost and fast convergence Gauss-Seidel pseudo affine projection algorithm for multichannel active noise control," in *Proc. 29th IEEE International Conference on Acoustics, Speech, and Signal Processing*, 2004, pp. 121-124.

[24] F. Yang, Y. Cao, M. Wu, F. Albu and J. Yang, "Frequency-domain filtered-x LMS algorithms for active noise control: A review and new insights," *Applied Science*, vol. 8, no.11, pp. 2313, 2018.

[25] K. Mazur, S. Wrona, and M. Pawelczyk, "Design and implementation of multichannel global active structural acoustic control for a device casing," *Mechanical Systems and Signal Processing*, vol. 98, pp. 877–889, 2018.

[26] C. Shi, Z. Jia, R. Xie, and H. Li, "An active noise control casing using the multi-channel feedforward control system and the relative path based virtual sensing method," *Mechanical Systems and Signal Processing*, vol. 144, p. 106878, 2020.

[27] B. Lam, D. Shi, W.-S. Gan, S. J. Elliott, and M. Nishimura, "Active control of broadband sound through the open aperture of a full-sized domestic window," *Scientific Reports*, vol. 10, no. 1, pp. 10021–10021, 2020.

[28] B. Lam, C. Shi, D. Shi, and W.-S. Gan, "Active control of sound through full-sized open windows," *Building and Environment*, vol. 141, pp. 16–27, 2018.

[29] C.-Y. Chang, A. Siswanto, C.-Y. Ho, T.-K. Yeh, Y.-R. Chen, and S. M. Kuo, "Listening in a noisy environment: Integration of active noise control in audio products," *IEEE Consumer Electronics Magazine*, vol. 5, no. 4, pp. 34–43, 2016.

[30] D. Shi, W.-S. Gan, B. Lam, and S. Wen, "Feedforward selective fixed-filter active noise control: Algorithm and implementation," *IEEE/ACM Transactions on Audio, Speech, and Language Processing*, vol. 28, pp. 1479–1492, 2020.

[31] S. R. Khosravirad, H. Viswanathan and W. Yu, "Exploiting diversity for ultra-reliable and low-latency wireless control," *IEEE Transactions on Wireless Communications*, vol. 20, no. 1, pp. 316–331, 2021.

[32] H. Zhang et al., "Scheduling with predictable link reliability for wireless networked control," *IEEE Transactions on Wireless Communications*, vol. 16, no. 9, pp. 6135–6150, 2017.

[33] L. Scheuvens, T. Hößler, P. Schulz, N. Franchi, A. N. Barreto and G. P. Fettweis, "State-aware resource allocation for wireless closed-loop control systems," *IEEE Transactions on Communications*, vol. 69, no. 10, pp. 6604–6619, 2021.

[34] P. Li, Y.-B. Zhao, and Y. Kang, "Integrated channel-aware scheduling and packet-based predictive control for wireless cloud control systems," *IEEE Transactions on Cybernetics*, 2020.

[35] P. Park, S. Coleri Ergen, C. Fischione, C. Lu, and K. H. Johansson, "Wireless network design for control systems: A survey," *IEEE Communications Surveys Tutorials*, vol. 20, no. 2, pp. 978–1013, 2018.

[36] G.-P. Liu, "Predictive control of networked multiagent systems via cloud computing," *IEEE Transactions on Cybernetics*, vol. 47, no. 8, pp. 1852–1859, 2017.

[37] X. Zheng, H. Zhang, H. Yan, F. Yang, Z. Wang and L. Vlacic, "Active full-vehicle suspension control via cloud-aided adaptive backstepping approach," *IEEE Transactions on Cybernetics*, vol. 50, no. 7, pp. 3113–3124, 2020.

[38] R. Galambos and L. Sujbert, "Active noise control in the concept of IoT," in *Proc. 16th International Carpathian Control Conference*, 2015, pp. 133–137.

[39] S. Shen, N. Roy, J. Guan, H. Hassanieh, and R. R. Choudhury, "MUTE: Bringing IOT to noise cancellation," in *Proc. 32nd Conference of the ACM Special Interest Group on Data Communication*, 2018, pp. 282–296.

[40] X. Shen, D. Shi, and W.-S. Gan, "A wireless reference active noise control headphone using coherence based selection technique," in *Proc. 46th IEEE International Conference on Acoustics, Speech and Signal Processing* , 2021, pp. 7983–7987.

[41] L. Sujbert, K. Molnár, G. Orosz, and L. Lajkó, "Wireless sensing for active noise control," in *Proc. 23rd IEEE Instrumentation and Measurement Technology Conference Proceedings*, 2006, pp. 123–128.

[42] C. Shi, Z. Yuan, R. Xie, and H. Li, "Simultaneous variable perturbation method for the active noise control system with a wireless error microphone," in *Proc. 12th Asia-Pacific Signal and Information Processing Association Annual Summit and Conference*, 2020, pp. 283–287.

[43] M. Ferrer, M. de Diego, G. Piñero and A. Gonzalez, "Affine projection algorithm over acoustic sensor networks for active noise control," *IEEE/ACM Transactions on Audio, Speech, and Language Processing*, vol. 29, pp. 448-461, 2021.

[44] Y. He, J. Guo and X. Zheng, "From surveillance to digital twin: Challenges and recent advances of signal processing for industrial Internet of Things," *IEEE Signal Processing Magazine*, vol. 35, no. 5, pp. 120–129, 2018.

[45] F. Tao, H. Zhang, A. Liu and A. Y. C. Nee, "Digital twin in industry: State-of-the-art," *IEEE Transactions on Industrial Informatics*, vol. 15, no. 4, pp. 2405–2415, 2019.

[46] R. Minerva, G. M. Lee and N. Crespi, "Digital twin in the IoT context: A survey on technical features, scenarios, and architectural models," *Proceedings of the IEEE*, vol. 108, no. 10, pp. 1785–1824, 2020.

[47] F. Yang, J. Guo and J. Yang, "Stochastic analysis of the filtered-x LMS algorithm for active noise control," *IEEE/ACM Transactions on Audio, Speech, and Language Processing*, vol. 28, pp. 2252-2266, 2020.

[48] Hangzhou Crysound Electronics Co., Ltd, "CRY333 Measurement microphone sets,"[Online]. Available: http://www.crysound.com/en/product/details/25.html

[49] Hangzhou Aihua Instruments Co., Ltd, "AWA5636-0 Sound Level Meter," [Online]. Available: https://www.hzaihua.com/products_cont.html?id=81